

# Photothermal Control of Heat-Shock Protein Expression at the Single Cell Level

Hadrien M. L. Robert,\* Julien Savatier, Stéphanie Vial, Jacob Verghese, Benoit Wattellier, Hervé Rigneault, Serge Monneret, Julien Polleux,\* and Guillaume Baffou\*

Laser heating of individual cells in culture recently led to seminal studies in cell poration, fusion, migration, or nanosurgery, although measuring the local temperature increase in such experiments remains a challenge. Here, the laser-induced dynamical control of the heat-shock response is demonstrated at the single cell level, enabled by the use of light-absorbing gold nanoparticles as nanosources of heat and a temperature mapping technique based on quadri-wave lateral shearing interferometry (QLSI) measurements. As it is label-free, this approach does not suffer from artifacts inherent to previously reported fluorescence-based temperature-mapping techniques and enables the use of any standard fluorescent labels to monitor in parallel the cell's response.

## 1. Introduction

Heating single cells in culture has attracted an increasing interest these last years due to several seminal studies pioneering nanosurgery,<sup>[1,2]</sup> cell poration,<sup>[3]</sup> cell fusion,<sup>[4]</sup> gene expression,<sup>[5]</sup> control of cell migration,<sup>[6]</sup> and neuronal spikes generation,<sup>[7,8]</sup> at the single cell level. All these studies contribute to the rise of two branches of research that could be named single-cell thermal

H. M. L. Robert, Dr. J. Savatier, Dr. S. Vial, Dr. H. Rigneault,  
Dr. S. Monneret, Dr. G. Baffou  
Institut Fresnel  
CNRS

Aix Marseille Univ  
Centrale Marseille, Marseille 13013, France

E-mail: hadrien.robert@fresnel.fr; guillaume.baffou@fresnel.fr

H. M. L. Robert, Dr. B. Wattellier  
PHASICS S.A.

Parc technologique de Saint Aubin  
Route de l'Orme des Merisiers  
91190 Saint Aubin, France

Dr. J. Verghese  
Max Planck Institute of Biochemistry  
Department of Cellular Biochemistry  
82152 Martinsried, Germany

Dr. J. Polleux  
Max Planck Institute of Biochemistry  
Department of Molecular Medicine  
82152 Martinsried, Germany  
E-mail: julienpolleux@googlemail.com

Dr. J. Polleux  
Center for NanoScience  
Ludwig Maximilian University  
80799 Munich, Germany

 The ORCID identification number(s) for the author(s) of this article can be found under <https://doi.org/10.1002/smll.201801910>.

DOI: 10.1002/smll.201801910

biology and thermogenetics. Some of these studies were inducing a temperature increase at the (sub)cellular level using a laser illumination under a microscope, where light absorption was due to the culture medium itself, or to nanoabsorbers, such as plasmonic (usually gold) nanoparticles dispersed at the vicinity of the cell, or on the inside.<sup>[3,4,6,9–15]</sup>

The main problem encountered by this branch of research is the difficulty to reliably measure a temperature increase in a medium as complex as the cytoplasm. A dozen of high spatial resolution tempera-

ture microscopy techniques were developed this last decade, suited for cellular imaging.<sup>[11,12,15–23]</sup> Most of them are optical techniques, and especially based on fluorescence imaging. Fluorescence is indeed a physical quantity that is highly temperature dependent. However, using fluorescence for this purpose has two drawbacks: i) it already takes a fluorescence spectral window for cell imaging, which makes any other fluorescence imaging of the cell more complicated and, ii) more importantly, it was recently evidenced that using fluorescence as a means to measure temperature in living cells was bound to create artefacts,<sup>[24,25]</sup> mostly because fluorescence properties (intensity, spectrum, life time, anisotropy) are not only temperature dependent. Many other factors affecting fluorescence can vary in the cytoplasm (pH, ionicity, viscosity, refractive index, etc.). For instance, some groups have reported endogenous (without any external heating) temperature variations inside single living cells by a few Kelvins, which were thought to be real, but which can be shown to be fully impossible by simple thermodynamic calculations.<sup>[17,26]</sup> Today, reliable and simple techniques are still lacking to enable these fields of research to blossom.

In this article, we demonstrate the ability of quadriwave lateral shearing interferometry, a label-free microscopy technique, to dynamically monitor the photothermal-induced expression of proteins at the single cell level. We also highlight the interests of using gold nanoparticles as nanosources of heat in these kinds of study. As an illustration, we studied the textbook case of the heat-shock response of living cells.

## 2. Results

### 2.1. Heat-Shock Proteins and Transcription Factors

In response to heat stress, triggered by a temperature increase of just a few degrees, cells activate a highly conserved, powerful

adaptation mechanism called the heat shock response (HSR). Cells rapidly alter their gene expression programs that results in the repression of protein biosynthesis and the induction of several cytoprotective genes encoding heat shock proteins (HSPs), thereby conferring resistance to heat shock and re-establishing protein homeostasis. Many HSPs function as molecular chaperones to protect thermally damaged proteins from misfolding and aggregating, and to refold and repair misfolded proteins or target them for degradation. Regulation of the HSR is mediated by heat shock transcription factors (HSFs), where HSF1 plays a primary role in the transcriptional regulation of HSP expression.<sup>[27]</sup>

Stress-dependent activation and transcriptional regulation mediated by HSF1 is a multistep process. Under normal conditions, inactive, monomeric HSF1, stabilized by interactions with molecular chaperones is predominantly located in the nucleus, but shuttling between the nucleus and cytoplasm has been reported.<sup>[28]</sup> Under stress conditions, active HSF1 forms trimers, binds to DNA with its activity regulated by extensive post-translational modifications. HSF1 binds to the promoters of HSF1 target genes, termed heat shock transcription elements (HSEs), which contain three to six inverted nucleotide repeats of the sequence  $nGAA_n$ , where  $n$  can be any nucleotide. A characteristic feature of the HSR is the binding of active HSF1 to linear satellite III repeats in chromosome 9 resulting in the formation of so-called nuclear stress granules.<sup>[29]</sup> The role of these stress granules is still unclear, but they correlate positively with the inducible transcriptional activity of HSF1 in the cell. By fluorescent labeling of HSF1, the formation of these granules within the nucleus can be easily visualized using confocal fluorescence microscopy and serve as an effective reporter of the cells response to heat-shock.<sup>[30,31]</sup>

## 2.2. System under Study

The system under study consisted of retinal pigmented epithelial (RPE) cells seeded on a dense array of gold nanoparticles (as sketched in **Figure 1a**) that can deliver heat upon laser illumination and locally increase the temperature. In RPE cells, HSF1 were fluorescently labelled by cell transfection (see Experimental Section, cell fluorescent labeling). Gold nanorods were synthesized in house and were subsequently immobilized onto a glass coverslip (see **Figure 1b** and Experimental Section, gold nanoparticle synthesis). This gold-nanoparticle functionalized coverslips were subsequently glued onto a perforated dish, and the RPE cells were cultured in it. Note that despite the nanometric nature of the sources of heat, the temperature does not consist on nanometric hot spots. The temperature is rather smooth and continuous over the illuminated area due to thermal homogenization effects, as if the heat source was a continuous micrometric hot plate.<sup>[32]</sup> Due to this effect, the extension of the temperature distribution is Gaussian-like and its typical size matches the size of the laser beam. In our experiments, the laser beam could range from 500 nm (focused mode) to a few tens of microns (in the unfocused configuration, see section Experimental Setup in the Experimental Section).

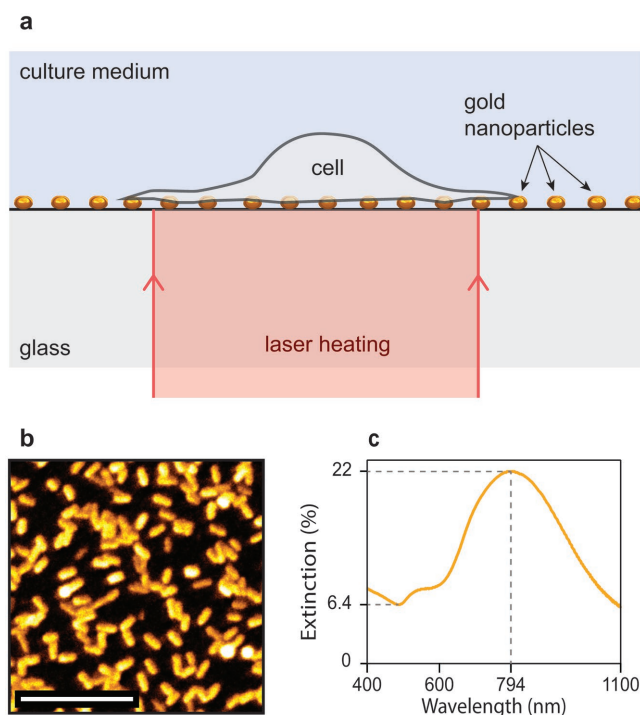


**Figure 1.** Description of the experimental approach. a) Schematic of the system under study: RPE cells adhered to a layer of gold nanoparticles (not to scale), which turn into heat sources under laser illumination. b) Scanning electronic microscopy (SEM) image of a gold nanoparticle substrate. Scale bar: 300 nm. c) Extinction spectrum of the coverslip functionalized with gold nanoparticles.

## 2.3. Temperature and Fluorescence Measurements

Quadriwave lateral shearing interferometry (QLSI) is an optical imaging technique based on the use of a wavefront sensing camera capable of mapping the spatial profile of an optical wavefront.<sup>[33–35]</sup> The camera consists of a regular CCD camera associated with a modified Hartmann diffraction grating attached to the camera at a millimetric distance from the CCD sensor. This configuration creates an interferogram that is further processed to retrieve the shape of the incoming wavefront on the camera. QLSI was used for two purposes in this work: i) as a quantitative phase imaging technique to image the cell morphology with high contrast,<sup>[36]</sup> as illustrated by **Figure 2a** (the wavefront distortion arises from the refractive index of the cell, different from the surroundings), ii) as a temperature microscopy technique as shown in **Figure 2b**. In this second configuration, the wavefront distortion comes from the temperature-induced variation of the refractive index of the heated medium. In a previous publication, we have shown how QLSI can be used to measure temperature profiles on the microscale.<sup>[37]</sup> We called this technique TIQSI for temperature imaging using QLSI. However, we have never used it before in a medium as complex as the interior of a living cell. The algorithm we used to retrieve the temperature profile from the wavefront distortion is described in a previous publication.<sup>[37]</sup> In any QLSI measurement, a first reference image has to be taken and subtracted to any image of interest to get rid of light beam imperfections.

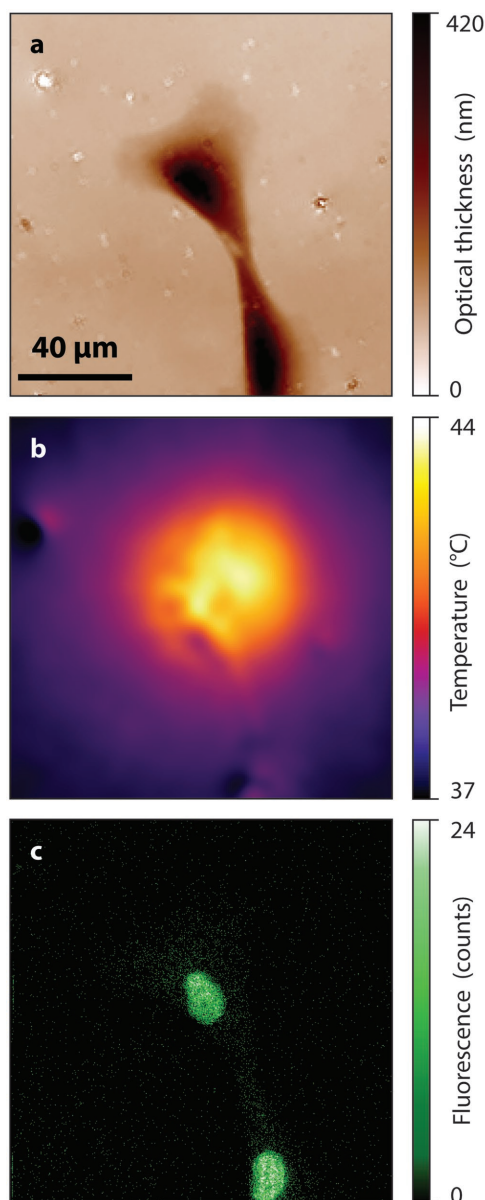


**Figure 2.** Presentation of the different imaging modalities of the experimental setup. a) QLSI image of two living RPE cells. b) Temperature distribution measured using QLSI when a laser, 50  $\mu\text{m}$  in diameter, is illuminating the cell. c) Fluorescence of the cell measured using confocal fluorescence microscopy, acquired in parallel with the temperature image. Scale bar for all images is shown in (a).

For cell imaging, this reference image is taken on a clear area (no cell over the field of view).<sup>[36]</sup> For temperature imaging, the reference image is taken exactly at the same location as the image of interest, i.e., with the cell of interest under the field of view, but with the heating laser off. This way, the wavefront distortion due to the presence of the cell goes in the reference image, and only the contribution of the temperature increase is measured. Since this technique is label-free, it offered us the possibility to conduct in parallel fluorescence measurements without any restriction on the fluorophore properties, as shown in Figure 2c. This way, three images can be acquired in

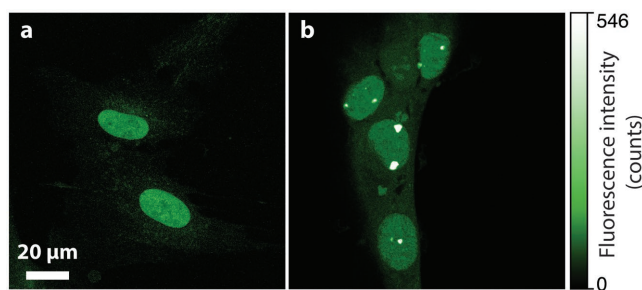


**Figure 3.** Fluorescence measurements in RPE cells as a function of the temperature. a) Fluorescence image of RPE cells at 37  $^{\circ}\text{C}$ . The fluorescence arises mainly from the nuclei and is rather uniform. b) Fluorescence image of RPE cells, resistively heated at 43  $^{\circ}\text{C}$  inducing the formation of fluorescent granules within the nucleus, a sign of cellular heat-shock response.

parallel: the cell morphology, the temperature distribution, and the distribution of HSF1 (see Figure 2).

The fact that the sources of heat are localized underneath the cells may result in a temperature gradient in the  $z$  direction throughout the cell. This effect can be reduced by increasing the laser beam diameter (see ref. [38], equation (7) for a detailed description). Note that attempt to achieve more uniform temperature profiles in the  $z$  direction by internalizing gold nanoparticles within the cell is not recommended, as it may create random, unknown, nonuniform nanoparticle distributions within the cell, different from one cell to another, or even uncontrolled aggregations. Moreover, internalizing nanoparticles is invasive and may disturb the cellular response of interest.

#### 2.4. Stress Activation in Single Cells

At 37  $^{\circ}\text{C}$ , the nuclei of RPE cells emit a rather uniform fluorescence, revealing a uniform nuclear distribution of HSF1 (see Figure 3a). Similarly to cells cultured 30 min in an incubator at 42–43  $^{\circ}\text{C}$ ,<sup>[30,39]</sup> fluorescent granules appeared in the illuminated cells under resistive heating, as observed in Figure 3b.

The most important benefit of heating single cells using laser illumination is the possibility to achieve fast dynamics on the subsecond time-scale. Figure 4 displays a series of successive images of RPE cells undergoing heating and cooling phases. In all these examples, a constant laser power was used to maintain a temperature of 43  $^{\circ}\text{C}$ . In less than a minute, granules appear and their contrast keeps on increasing during a few minutes. Figure 4a shows two cells where only the heated cell (in the middle of the image) displays granules, while the cell that is not heated, a few tens of  $\mu\text{m}$  away, does not undergo any stress response (no granule appears). These trindoductory results evidence the possibility to activate the stress response in single cells upon laser heating, reproducing the observation conducted on large populations of cells with macroscopic resistive heating.

Figure 5 plots the evolution of the granules' fluorescence as a function of time for a single cell, as a means to monitor the heat-shock response of the cell. Three different laser intensities have been applied for 2 min (4, 8, and 12 mW) corresponding

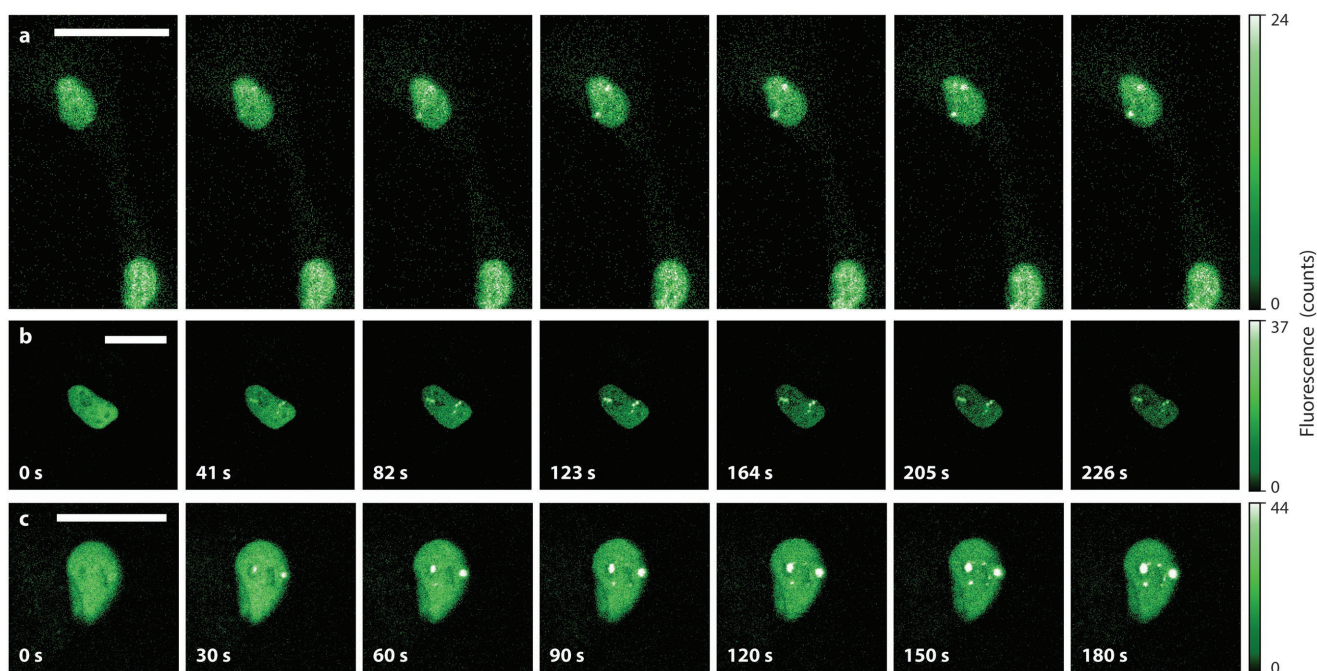


**Figure 4.** Monitoring of the heat-shock response of three living cells a–c) heated at 44 °C. After around 1 min of heating, a couple of stress granules appear in the nuclei. In case (a), only the upper cell was illuminated. Scale bars: 40  $\mu$ m.

to temperatures of 39, 42, and 44 °C. The successive heatings were spaced by 1 min intervals. Each time, granules appeared at the same position within the nucleus. Interestingly, the rise-time of the heat-shock response does not seem to depend on the laser power, i.e., on the magnitude of the stress. During the laser heating phase, in Figure 5b, the three line shapes overlap. Such an observation is consistent with a dynamics governed by the ribosome transcription speed, which is weakly temperature dependent. However, the heat-shock response neither stop nor even decrease when the heat stress is stopped. It may keep on progressing over a much longer time scale than the heating duration, especially for large temperature increase (case 42 °C). This observation shows that the transcription factor does not stop its activity when the stimulus disappears, but later, presumably when all the unfolded proteins have been repaired. This hypothesis will be further tested in a future study, where statistics will be carried out over a large amount of cells. Note that the dynamics of the granule disappearance also seem constant over the investigated range of temperature. This overall time scale of the heat-shock response of a few minutes is consistent with previous studies.<sup>[40]</sup>

### 3. Discussion

The experimental approach introduced in this article cumulates four main advantages compared to other reported approaches, as listed hereinafter.

First, TIQSI does not suffer from the inherent artifacts of fluorescence-based techniques<sup>[24,25]</sup> and offers full flexibility on the use of fluorescence staining to observe other parameters of interest in the cells. This is what we illustrated with the HSF

monitoring. Moreover, QLSI is fast (a few seconds per image in our case or even less depending of the camera).

Then, laser heating is the most natural and advantageous approach when microscale heating is desired in a transparent sample. It enables the remote heating over any area of the sample down to around 500 nm. This would not be possible using resistive heating of microwires for instance. Then, using gold nanoparticles as the absorbing medium offers three benefits: i) when illuminating a single nanoparticle (not a dense carpet of nanoparticles), the size of the heated area can be reduced to the size of the nanoparticle. This benefit has been widely used in photothermal microscopy.<sup>[41]</sup> ii) The gold-nanoparticle samples we used can be fabricated using a simple chemical approach. On the contrary, depositing an absorbing metal layer requires bulky, expensive apparatus. iii) The only interaction that exists between gold nanoparticles and light is absorption. Scattering is negligible if the nanoparticles are small enough<sup>[9]</sup> and reflection does not exist, unlike with a metal layer. Using a metal layer would thus yield a less efficient heating and would even strongly damp the collected fluorescence. This drawback is reduced using gold nanoparticles because they can be made resonantly absorbent only in the IR region and not in the visible region. This way, they will efficiently absorb the infrared laser, but not the emitted fluorescence (see Figure 1d).

Moreover, compared to overall resistive sample heating, heating a reduced volume yields a reduced thermal inertia that enables faster temperature variations. When heating a single cell, say 10  $\mu$ m big, the variations of the temperature can be as fast as  $\approx$ 1 ms.<sup>[42]</sup> This is much faster than any cell response to temperature variations. Thus, temperature variations can be considered as instantaneous for the cell and the reference time

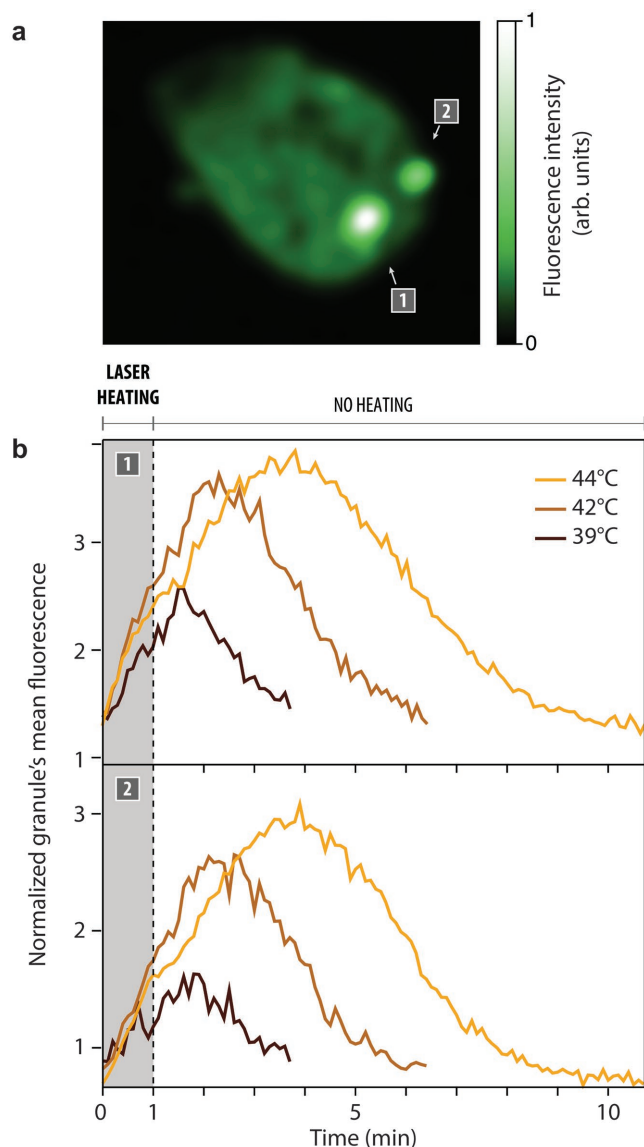


**Figure 5.** Dynamics of the heat-shock response of a single cell at different temperatures. a) Fluorescence imaging showing two nuclear stress granules upon heating at 44 °C. The image has been smoothed using a Gaussian convolution for the sake of clarity. b) Evolution of the mean fluorescence of the two granules as a function of time for three successive and different 1 min heating conditions: 44, 42, and 39 °C (heating laser diameter: 40  $\mu\text{m}$ ). One fluorescence image was taken every 6 s.

$t = 0$  is perfectly defined. This way, rapid processes can be quantitatively monitored, as illustrated in Figure 5. This also offers the ability to precisely study the couple of physical quantities time–temperature. Indeed, not only the temperature increase but also its duration are important when dealing with a heat-induced cell damage for instance.<sup>[43]</sup>

Finally, when heating individual cells, one can simply either stress the cell in a physiological range of temperature values or injure it above 43 °C. This enables the investigation of the response of one cell or more cells to hazardous temperature–time conditions, without taking the risk to affect or even kill the whole population of the sample. Thus, this approach can

be time-saving regarding the number of samples that have to be prepared, with a higher throughput for a serial experiments. More importantly, this approach enables the heating of subcellular compartments, by focusing the laser instead of expanding it over the whole cell area. Investigating the heat-shock response of single cells when focusing the laser at the submicrometric scale will be the purpose of a next study.

## 4. Conclusion

To summarize, in this work, we monitored for the first time the photothermal-induced heat-shock response of cells in culture at the single cell level, and demonstrate how this task can be efficiently achieved using a synergetic approach based on i) temperature imaging using wavefront sensing and ii) gold nanoparticles as nanosources of heat.

Compared to a global resistive heating of the sample, our approach presents numerous benefits: i) It enables the study of subsecond time scales. ii) It is label-free and thus noninvasive (no need to tag the cells with temperature-sensitive fluorescent molecules). iii) It is not fluorescence-based, which implies that no constraint limits the choice of fluorescent labels to monitor the cell's response. iv) Subcellular compartments can be heated, offering the possibility to address new biological relevant questions related to cellular stress mechanisms.

We hope this study could favor the development of a nascent field of research called thermal biology at the single cell level.

## 5. Experimental Section

**Experimental Setup:** The experimental setup used to perform laser heating on the microscale and acquire the fluorescence and temperature images of living cells is sketched in Figure 6. A Köhler illumination (KI) was positioned on top of the sample, illuminating the sample with a light emitting diode at  $625 \pm 9$  nm (Thorlabs M625L3). The sample was composed of a glass bottom dish containing the cells and inserted in a Chalmide microscope stage incubator (TS) that regulates sample temperature (at 37 °C) and  $\text{CO}_2$  partial pressure. Two Olympus immersion-oil microscope objective lenses (MO) were used (100 $\times$ , 1.35NA and 40 $\times$ , 1.3NA). A standard confocal microscopy configuration was implemented to construct fluorescence images. It was composed of a 488 nm laser, two fast galvanometric scanning mirrors (fSM) and an avalanche photodiode (APD). Confocal images were acquired using an original Labview program developed by Patrick Ferrand<sup>[44]</sup> and further adapted following the needs. Heating was performed using a Ti:Sapph laser (Millenia-Tsunami, Spectraphysics). The laser wavelength could be shifted from 710 to 880 nm to match the plasmonic resonance frequency of the gold nanoparticles. In the presented results, it was set at 785 nm. A manual rotative mirror was used to adjust the position of the laser spot on the sample, in the case of focalized heating. To heat over an extended area, much larger than the diffraction limit, the flip lens (FL) was removed so that the laser was focused in the entrance pupil of the objective lens (MO). This configuration produced a uniform laser illumination, the diameter of which could be adjusted up to a few tens of micrometers using the diaphragm (D). In the results presented in the manuscript, only the uniform illumination was used and the beam diameter was set to 50  $\mu\text{m}$ .

**Temperature Image Processing Using QLSI:** Temperature images were processed using the linear version of the algorithm described in the previous work.<sup>[37]</sup> A Tikhonov parameter  $\alpha = 10^{-3}$  was used in order to remove the noise stemming from the deconvolution algorithm, and

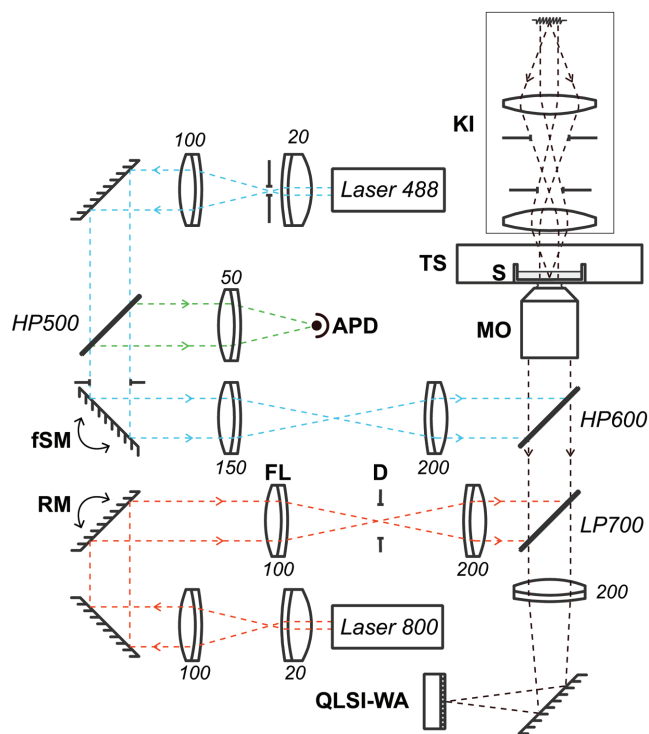


**Figure 6.** Microscopy setup used to perform laser heating on the micro-scale and acquire the fluorescence and temperature images of living cells. KI: Köhler illumination; TS: thermal stage; MO: microscope objective lens; HPxxx, LPxxx: High-pass, low-pass filters centered at xxx nm; RM: Manual rotative mirror; D: diaphragm; FL: flipping lens; FSM: fast-scanning mirrors; QSI-WA: QLSI wavefront sensing camera; APD: avalanche photodiode.

to reduce the imperfections of the image due to the presence of the cell. The temperature maps and temperature values were measured  $z = 3 \mu\text{m}$ , to better reflect the temperature inside the cell, and not at the glass/water interface. When global cell temperatures are specified in the manuscript (like 39, 41 and 44 °C), they consist of a temperature averaged over a square area of  $30 \times 30 \mu\text{m}^2$ .

**Gold Nanoparticle Sample Fabrication: Nanorods Synthesis Protocol:** Material: Tetrachloroauric acid ( $\text{HAuCl}_4$ ,  $3\text{H}_2\text{O}$ ), sodium borohydride, silver nitrate,  $\text{HCl}$ ,  $\text{NH}_4\text{OH}$  (32%), poly-(styrenesulfonate) (PSS,  $M_w$  70 000, 20 wt%) and poly(diallyldimethylammonium chloride) (PDDA,  $M_w < 100$  000), were purchased from Aldrich. Poly(vinylpyrrolidone) (PVP,  $M_w$  40 000) was supplied by Fluka. Ascorbic acid, sodium chloride ( $\text{NaCl}$ ), cetyltrimethyl ammonium bromide (CTAB), PDPA ( $M_w$  100 000, 20 wt%) were procured from Sigma. All chemicals were used as received. 96% pure isopropanol and Milli-Q grade water were used to prepare all solutions.

**Gold Nanoparticle Sample Fabrication: Preparation of Gold Nanorods Solutions:** The gold nanorods synthesis is adapted from the protocols developed by Nikoobakht et al.<sup>[45]</sup> and Liu et al.<sup>[46]</sup>

All the glassware were first cleaned with an aqua regia solution ( $\text{HCl}/\text{HNO}_3=70/30$ ) for 5 min, then washed with Milli-Q water and isopropanol and dried.

The gold seeds were synthesized by borohydride reduction of  $0.28 \times 10^{-3} \text{ M HAuCl}_4$  in an aqueous 0.1 M CTAB solution. 76  $\mu\text{L}$  of the seed solution was added to the following growth solution (8 mL): 0.1 M CTAB,  $0.5 \times 10^{-3} \text{ M HAuCl}_4$ ,  $0.8 \times 10^{-3} \text{ M}$  ascorbic acid, and silver nitrate ( $0.08 \times 10^{-3} \text{ M}$ ). The solution was then stored at 30 °C overnight.

Then, the as-prepared gold nanorods were functionalized with PVP. The excess of CTAB was discarded by centrifugation (8000 rpm, 20 min) and the gold nanorods were resuspended in Milli-Q water. The solution of the gold nanorods was added dropwise to a solution of PVP ( $10 \text{ g L}^{-1}$ )

under vigorous stirring and leave overnight under gentle stirring. The PVP-functionalized gold nanorods were washed by centrifugation at 4000, 5000, and 7000 rpm for 10 min. The supernatant was discarded and the particles were redispersed in isopropanol under sonication.

**Gold Nanoparticle Sample Fabrication: Coverslip Functionalization:** Before the deposition of the PVP-functionalized gold nanorods onto the surface of the coverslip, the latter has been recovered by 3 layers of polyelectrolytes as described in the work of Vial et al.<sup>[47]</sup> 170  $\mu\text{m}$  thick glass coverslips were first cleaned using base piranha solutions. Each coverslip was immersed for 20 min in a solution of PDPA ( $1 \text{ g L}^{-1}$ , 0.5 M of  $\text{NaCl}$ ), then 10 min in a solution of PSS ( $1 \text{ g L}^{-1}$ , 0.5 M of  $\text{NaCl}$ ) and finally 10 min in a solution of PDPA ( $1 \text{ g L}^{-1}$ , 0.5 M of  $\text{NaCl}$ ). Between each layer, the coverslip was rinsed with water and dried under  $\text{N}_2$  stream.

**Gold Nanoparticle Sample Fabrication: Nanorods Deposit:** The functionalized coverslips were immersed in a solution of PVP-gold nanorods for 3 h. The deposition was promoted via electrostatic interactions between the positively charged coverslip and the negatively charged gold nanorods. The slides were then rinsed with Milli-Q water and dried. In order to have only one side of the slide covered with nanoparticles, the other side was cleaned with a tissue soaked with ethanol.

**Cell Culture:** Transient transfection of cells was done using Lipofectamine 2000 reagent (Invitrogen) according to the manufacturer's protocol. We used 2  $\mu\text{g}$  DNA of HSF-1-enhanced green fluorescence protein (EGFP) construct for transfection in 6-well format. Human HSF-1 was cloned into the vector pEGFP-N2, with the EGFP at the C-terminal. HSF-1 was cloned into the vector using the restriction enzymes Bgl II and Kpn I.<sup>[48]</sup> The transfection reagent and DNA were diluted in Opti-MEM medium and were added to DMEM:F12 medium (without penicillin-streptomycin solution). After an incubation of 4–6 h in presence of cells, the medium was replaced by fresh DMEM medium (without penicillin-streptomycin).

RPE1 cells were maintained in Dulbecco's modified Eagle's medium (DMEM:F12; Gibco) supplemented with 10% fetal bovine serum (FBS), 1% penicillin-streptomycin (Gibco) and 1% L-glutamine (Gibco) at 37 °C in an atmosphere of 5%  $\text{CO}_2$ . To take cells in suspension they were washed with PBS and incubated with 2 mL of a trypsin/ethylenediaminetetraacetic solution for 2 min at 37 °C until cells detached from the substrate. After being collected, the cells were centrifuged (5 min, 600  $\times$  g). The cell-pellet was resuspended in growth medium, counted and seeded onto gold nanoparticle-based substrates.

Prior to the optical experiments, cells are rinsed, immersed in a Leibovitz's L-15 (Gibco) medium, without phenol red and a buffer solution. To favor cell adhesion, a poly-L-lysine coating was done on the gold nanoparticle substrate.

## Acknowledgements

This work was supported by the Agence Nationale de la Recherche (Grant PlasmTherm, ANR-15-CE24-0025-01). HMLR's Ph.D. grant was partially financed by the Agence Nationale de la Recherche et de la Technologie (ANRT) through the CIFRE program. The authors thank Jerome Wenger for providing the facilities for SEM imaging.

## Conflict of Interest

H.M.L.R. is a Ph.D. student with a financial support that partly came from Phasics company. B.W. is a member of the Phasics Company.

## Keywords

cell imaging, gold nanoparticles, heat-shock, photothermal, plasmonics

Received: May 18, 2018

Revised: June 6, 2018

Published online: July 11, 2018

- [1] A. Vogel, J. Noack, G. Hüttman, G. Paltauf, *Appl. Phys. B* **2005**, *81*, 1015.
- [2] R. Lachaine, C. Boutopoulos, P. Y. Lajoie, E. Boulais, M. Meunier, *Nano Lett.* **2016**, *16*, 3187.
- [3] M. Li, T. Lohmüller, J. Feldmann, *Nano Lett.* **2015**, *15*, 770.
- [4] A. Bahadori, L. B. Oddershede, P. M. Bendix, *Nano Res.* **2017**, *10*, 2034.
- [5] P. Ginet, K. Montagne, S. Akiyama, A. Rajabpour, A. Taniguchi, T. Fujii, Y. Sakai, B. Kim, D. Fourmy, S. Volz, *Lab Chip* **2011**, *11*, 1513.
- [6] M. Zhu, G. Baffou, N. Meyerbröker, J. Polleux, *ACS Nano* **2012**, *6*, 7227.
- [7] F. Lavoie-Cardinal, C. Salesse, E. Bergeron, M. Meunier, P. De Koninck, *Sci. Rep.* **2016**, *6*, 20619.
- [8] Y. G. Ermakova, A. A. Lanin, I. V. Fedotov, M. Roshchin, I. V. Kelmanson, D. Kulik, Y. A. Bogdanova, A. G. Shokhina, D. S. Bilan, D. B. Staroverov, P. M. Balaban, A. B. Fedotov, D. A. SidorovBiryukov, E. S. Nikitin, A. M. Zheltikov, V. V. Belousov, *Nat. Commun.* **2017**, *8*, 15362.
- [9] G. Baffou, R. Quidant, *Laser Photonics Rev.* **2013**, *7*, 171.
- [10] A. Kyrsting, P. M. Bendix, D. G. Stamou, L. B. Oddershede, *Nano Lett.* **2011**, *11*, 888.
- [11] J. S. Donner, S. A. Thompson, M. P. Kreuzer, G. Baffou, R. Quidant, *Nano Lett.* **2012**, *12*, 2107.
- [12] G. Kucsko, P. C. Maurer, N. Y. Yao, M. Kubo, H. J. Noh, P. K. Lo, H. Park, M. D. Lukin, *Nature* **2013**, *500*, 54.
- [13] L. Shang, F. Stockmar, N. Azadfar, G. U. Nienhaus, *Angew. Chem., Int. Ed.* **2013**, *52*, 11154.
- [14] T. Tsuji, S. Yoshida, A. Yoshida, S. Uchiyama, *Anal. Chem.* **2013**, *85*, 9815.
- [15] L. Yang, H.-S. Peng, H. Ding, F. T. You, L. L. Hou, F. Teng, *Microchim. Acta* **2014**, *181*, 743.
- [16] V. Zeeb, M. Suzuki, S. Ishiwata, *J. Neurosci. Methods* **2004**, *139*, 69.
- [17] M. Suzuki, V. Tseeb, K. Oyama, S. Ishiwata, *Biophys. J.* **2007**, *92*, L46.
- [18] C. Gota, K. Okabe, T. Funatsu, Y. Harada, S. Uchiyama, *J. Am. Chem. Soc.* **2009**, *131*, 2766.
- [19] L. Martinez Maestro, E. Martín Rodríguez, F. Sanz-Rodríguez, M. C. Iglesias-de la Cruz, A. Juarraz, R. Naccache, F. Vetrone, D. Jaque, J. A. Capobianco, J. García Solé, *Nano Lett.* **2010**, *10*, 5109.
- [20] F. Vetrone, R. Naccache, A. Zamarrón, A. Juarraz de la Fuente, F. Sanz-Rodríguez, L. Martinez Maestro, E. Martín Rodríguez, D. Jaque, J. García Solé, J. A. Capobianco, *ACS Nano* **2010**, *4*, 3254.
- [21] K. M. McCabe, E. J. Lacherndo, I. Albino-Flores, E. Sheehan, M. Hernandez, *Appl. Environ. Microbiol.* **2011**, *77*, 2863.
- [22] J. Yang, H. Yang, L. Lin, *ACS Nano* **2011**, *5*, 5067.
- [23] K. Okabe, N. Inada, C. Gota, Y. Harada, T. Funatsu, S. Uchiyama, *Nat. Commun.* **2012**, *3*, 705.
- [24] G. Baffou, H. Rigneault, D. Marguet, L. Jullien, *Nat. Methods* **2014**, *11*, 899.
- [25] G. Baffou, H. Rigneault, D. Marguet, L. Jullien, *Nat. Methods* **2015**, *12*, 803.
- [26] S. Kiyonaka, T. Kajimoto, R. Sakaguchi, D. Shinmi, M. Omatsu-Kanbe, H. Matsuura, H. Imamura, I. Yoshizaki, I. Hamachi, T. Morii, Y. Mori, *Nat. Methods* **2013**, *10*, 1232.
- [27] M. Akerfelt, R. I. Morimoto, L. Sistonen, *Nat. Rev. Mol. Cell Biol.* **2010**, *11*, 545.
- [28] P. A. Mercier, N. A. Winegarden, J. T. Westwood, *J. Cell Sci.* **1999**, *112*, 2765.
- [29] C. Jolly, L. Konecny, D. L. Grady, Y. A. Kutsikova, J. J. Cotto, R. I. Morimoto, C. Vourc'h, *J. Cell Biol.* **2002**, *156*, 775.
- [30] J. J. Cotto, S. G. Fox, R. I. Morimoto, *J. Cell Sci.* **1997**, *110*, 2925.
- [31] T. P. Alastalo, M. Hellesuo, A. Sandqvist, V. Hietakangas, M. Kallio, L. Sistonen, *J. Cell Sci.* **2003**, *116*, 3557.
- [32] G. Baffou, P. Berto, E. Bermúdez Ureña, R. Quidant, S. Monneret, J. Polleux, H. Rigneault, *ACS Nano* **2013**, *7*, 6478.
- [33] J. Primot, L. Sogno, *J. Opt. Soc. Am. A* **1995**, *12*, 2679.
- [34] J. Primot, N. Guérineau, *Appl. Opt.* **2000**, *39*, 5715.
- [35] S. Velghe, J. Primot, N. Guérineau, M. Cohen, B. Wattellier, *Opt. Lett.* **2005**, *30*, 245.
- [36] P. Bon, G. Maucort, B. Wattellier, S. Monneret, *Opt. Express* **2009**, *17*, 13080.
- [37] G. Baffou, P. Bon, J. Savatier, J. Polleux, M. Zhu, M. Merlin, H. Rigneault, S. Monneret, *ACS Nano* **2012**, *6*, 2452.
- [38] G. Baffou, E. Bermúdez Ureña, P. Berto, S. Monneret, R. Quidant, H. Rigneault, *Nanoscale* **2014**, *6*, 8984.
- [39] H. G. Park, S. I. Han, S. Y. Oh, H. S. Kang, *Cell. Mol. Life Sci.* **2005**, *62*, 10.
- [40] C. Jolly, Y. Usson, R. I. Morimoto, *Proc. Natl. Acad. Sci. USA* **1999**, *96*, 6774.
- [41] D. Lasne, G. A. Blab, S. Berciaud, M. Heine, L. Groc, D. Choquet, L. Cognet, B. Lounis, *Biophys. J.* **2006**, *91*, 4598.
- [42] G. Baffou, H. Rigneault, *Phys. Rev. B* **2011**, *84*, 035415.
- [43] J. Overgaard, H. D. Suit, *Cancer Res.* **1979**, *39*, 3248.
- [44] P. Ferrand, *Comput. Phys. Commun.* **2015**, *192*, 342.
- [45] B. Nikoobakht, M. A. El-Sayed, *Chem. Mater.* **2003**, *15*, 1957.
- [46] M. Liu, P. Guyot-Sionnest, *J. Phys. Chem. B* **2004**, *108*, 5882.
- [47] S. Vial, I. Pastoriza-Santos, J. Pérez-Juste, L. M. Liz-Marzán, *Langmuir* **2007**, *23*, 4606.
- [48] Vector for fusing EGFP to the C-terminus of a partner protein, (accessed: March 2018).